Materials & Design 261 (2026) 115277

Contents lists available at ScienceDirect

Materials & Design

journal homepage: www.elsevier.com/locate/matdes

Functional elongational and adhesive strategies in the microstructured exoskeleton of the kissing bug *Mepraia spinolai*

Nicolás Padilla-Manzano [a,b,*], Lisa Shafroth [c], Laura Tamayo [a], Nicol Quiroga [b], Carezza Botto-Mahan [b], Francisco Melo [d,**]

[a] Departamento de Química, Facultad de Ciencias, Universidad de Chile, Las Palmeras 3425, Casilla 653, Santiago, Chile
[b] Departamento de Ciencias Ecológicas, Facultad de Ciencias, and Research Ring in Pest Insects and Climatic Change (PIC^2), Universidad de Chile, Las Palmeras 3425, Casilla 653, Santiago, Chile
[c] Ecole Polytechnique, Route de Saclay, 91120 Palaiseau, France
[d] Departamento de Física, Facultad de Ciencia, Universidad de Santiago de Chile, and Center for Soft Matter Research, SMAT-C, Av. B. O'Higgins 3363, Santiago, Chile

ARTICLE INFO

Keywords:
Composite
Exoskeleton
Stretchable
Microstructure
Adhesive
Biomechanics

ABSTRACT

Adverse and unpredictable environmental conditions constrain feeding and survival in wildlife. In the kissing bug *Mepraia spinolai*, the abdominal exoskeleton plays a key role in sustaining the extraordinary feeding capacity of the nymphal stages. Our results show that the exoskeleton is a layered composite showing a material gradient. The stretchable capacity is attributed to micro-wrinkles and micropillars located in the exocuticle, which covers a softer and thicker endocuticle. Moreover, the epicuticle exhibits weak adhesive properties that enable the attachment of a thin granular film. This loosely adhered layer, supported by the wrinkled substrate, expands easily and prevents strong adhesion of large particles. Altogether, these findings highlight how hierarchical structural design and compositional gradients confer *M. spinolai*'s exoskeleton with extraordinary expandability without compromising protection, offering insights into bioinspired strategies for designing multifunctional structural materials with tunable mechanical responses.

1. Introduction

Structured biological materials are an interesting example of different types of adaptations to the environment. These materials are complex matrices of organic and inorganic compounds such as chitin, collagen, calcite, and hydroxyapatite [1]. The material's chemical and mechanical profile, as well as its auto-assembly process and hierarchical structuring, contribute to its peculiar characteristics, including improved flexibility, toughness, roughness, strength, and crucial properties in response to adverse environments. Therefore, these materials can be fundamental in sustaining the existence of living organisms [2–5].

Arthropods are living examples of versatile biological materials. For instance, the presence of an exoskeleton, an external composite of organic and inorganic compounds structured even at the nano- and microscale, acts like a first barrier that not only delimits the boundary of this complex system from its environment but also provides locomotion, mechanics, camouflaging, and other functions to this group of animals [6]. Previous studies have attempted to understand the exoskeleton structural design and its chemical and mechanical properties in several arthropods, such as crabs [7–9], lobsters [10], shrimps [11], spiders [12,13], scorpions [14,15], isopods [16,17], and even in insects that present their exoskeleton as a layered cuticle [18–22].

Triatomine species (Hemiptera: Reduviidae: Triatominae), commonly known as kissing bugs, are strict blood-sucking insects widely distributed in diverse environments across the Americas, ranging from tropical rainforests to arid and semiarid regions [23]. Their developmental cycle includes the egg, five successive immature stages (nymphs) with rudimentary wings in later stages, and male and female adults [24]. Kissing bugs require few but relatively substantial blood meals to complete their development, which are obtained from various vertebrate species included in their diet [25]. Some triatomine species exhibit different strategies that allow them to expand their abdomen during the ingestion of large amounts of blood and that involve changes in the connexivum described mainly in adults [26]; however, the strategies adopted by nymphs have been poorly studied. The exoskeleton that

* Corresponding author at: Departamento de Química, Facultad de Ciencias, Universidad de Chile, Las Palmeras 3425, Casilla 653, Santiago, Chile.
** Corresponding author at: Departamento de Física, Facultad de Ciencia, Universidad de Santiago, Avenida Victor Jara 3493, Santiago, Chile
E-mail addresses: nicolas.padilla.m@ug.uchile.cl (N. Padilla-Manzano), francisco.melo@usach.cl (F. Melo).

https://doi.org/10.1016/j.matdes.2025.115277
Received 5 September 2025; Received in revised form 4 December 2025; Accepted 4 December 2025
Available online 10 December 2025

allows abdomen expansion was described through the observation of SEM images of different species as a micro-sculptured wrinkled, or, in some cases, striated surface [26]. Studying triatomine bugs is relevant as they serve as vectors for the protozoan *Trypanosoma cruzi*, the causative agent of Chagas disease, which is one of the most neglected vector-borne diseases in America [27].

Mepraia spinolai is a sylvatic triatomine bug endemic to Chile. It can be found in arid and semi-arid Mediterranean ecosystems (26°-33° S), including the Atacama Desert, and covering a wide climatic variation [28,29]. Therefore, *M. spinolai* is probably a species adapted to adverse environmental conditions because of daily and seasonal thermal variations with scarce and unpredictable rainfall, where potential blood meals can exhibit extreme fluctuations depending on the vegetation cover [30]. Unlike most triatomine species, *M. spinolai* are active during the day and nymphs exhibit a marked camouflaging behavior, actively using their third pair of legs to cover their complete body with dirt grains right after molting from one developmental stage to the next [31,32]. Dirt grains remain adhered to the *M. spinolai* exoskeleton until the next molting event, and the grains are even kept on the exuvia (i.e., the molted exoskeleton). Camouflage provides several advantages for *M. spinolai*, such as predator avoidance and/or undetected foraging, and individuals of this species employ lurking and stealthy approaches to unaware prey [32,33]. In terms of its ecology, *M. spinolai* sylvatic individuals can undergo several months of fasting throughout the year, increasing their feeding opportunities during late spring and summer when vertebrates (mammals, birds, and lizards) are more abundant [33]. A field study conducted by Estay-Olea et al. [34] in the central region of the *M. spinolai* distribution (31° S) showed a highly variable nutritional condition among individuals, suggesting that feeding opportunities are probably scarce and temporarily limited in this ecosystem. In this species, nymphs enlarge and shrink their abdomens due to bulky feeding events that have not been studied yet. In the present study, we provide insights into the aspects related to the material that sustains the lifestyle of *M. spinolai* populations. Specifically, we focus on its exoskeleton, which we show is a highly stretchable, microstructured, and hierarchical material covered by a thin and adhesive viscoelastic layer. We studied the chemical compositional design of this material by ATR-FTIR spectroscopy, TGA, and CLSM by means of cuticle autofluorescence to visualize the hierarchical structure. To elucidate the feeding capacity of this population, we analyzed the feeding data from nymphs, which is strongly related to a high stretching of their abdomen. The extraordinary feeding capacity of *M. spinolai* individuals allows them to survive despite long periods of starvation, which is suggested to be related to the presence of micro wrinkles and a network of micropillars that allow great expansion of their abdomens. Three main elements composing the *M. spinolai* abdominal exoskeleton are identified, namely, a soft inner layer (endocuticle), a thinner but rigid outer layer (exocuticle), and a thin and sticky outermost soft layer (epicuticle). We investigated the main elastic parameters of the abdominal exoskeleton, i.e., Young's modulus of the endocuticle and the exocuticle, through nanoindentation methods. Our results suggest that the wrinkle structure is dictated by the optimization of total elastic energy, which considers both the bending energy of the rigid exocuticle and the stretching energy of the endocuticle. The adhesion of the epicuticle was evaluated through the analysis of force–displacement curves obtained by atomic force microscopy (AFM), revealing that the adhesion energy is small but sufficient to support the weight of typical soil or dirt grains and allows easy expansion of the granular layer. Altogether our work could be relevant in bioinspired composites and hierarchical materials, as this cuticle embody design principles that link composition, hierarchical structure, and mechanical performance as a functional material [3,35–38]. Insects have developed lightweight yet robust exoskeletons capable of combining stiffness, toughness, and flexibility through controlled gradients in material composition and architecture. Understanding nature's strategies after millions of years of evolution by natural selection provides valuable insights for the rational design of bioinspired structural materials, particularly those requiring optimized strength-to-weight ratios, adaptability, and multifunctionality [36–40]. As advances in imaging and mechanical characterization continue to uncover the fine-scale organization of these materials, insect cuticles emerge as powerful models for developing next-generation bioinspired materials with tunable mechanical properties [41–43].

2. Materials and methods

2.1. Materials

Sodium cacodylate trihydrate ≥ 98 %, Sodium Chloride ReagentPlus ≥ 99 %, and Glutaraldehyde 25 % Aqueous Solution ≥ 98 % (TLC) were purchased from Sigma-Aldrich. Ethanol ≥ 99.5 % was purchased from Winkler. Deionized water with a resistivity of 18.2 MΩcm, a conductivity of 0.055 μS/cm, and a total organic carbon (TOC) content of less than 10 ppb was obtained from a LabStar 4-DI.

2.2. Specimen collection, conditions, and ethics

M. spinolai specimens were collected from interior valleys of the semiarid-Mediterranean ecosystem of central Chile (30° 51′ − 32° 38′ S). Adults were used to rear parasite-free laboratory colonies under optimal growing conditions (27–28 °C and 70–80 % RH) and fed as previously reported [44]. The nymphs IV and V (late nymphs hereafter) obtained from these crossings were used in the procedures explained in the next subsections due to their availability and size for better manipulation. Exuviae of molten exoskeletons were collected through the development process and were used in the procedure indicated in subsection 2.4. For comparison to laboratory-reared, wild late nymphs were also used to evaluate their adhesive properties following the procedure explained in subsection 2.7.

The Institutional Animal Care and Use Committee (CICUA) of University of Chile reviewed and approved the animal handling protocols used in this study (Certificate No. 22553-FCS-UCH-e5). The Local Biosafety Committee of the Faculty of Sciences of University of Chile granted the Biosafety Certificate (2022_CLB_FC_UCH_017).

2.3. Relative weight increase after the feeding process

Data from an F1 colony of *M. spinolai* were analyzed, with permission, from a previous report to determine weight gain through blood engorgement of late nymphs [45]. Parental insects were collected in the same semi-arid zone as our work, the F1 reared specimens were weighed before (W_i) and after (W_f) feeding on *Mus musculus* blood until engorgement (physiological satiety). Relative weight increase (Wt%) was calculated as follows:

$$Wt\% = \frac{W_f - W_i}{W_i} * 100$$

2.4. Chemical profile of M. spinolai exoskeleton

Attenuated total reflection-Fourier transform infrared analysis (ATR-FTIR)

The spectra of late nymphs with and without adhered grains were performed in random parts (5 zones) of dorsal abdomen section surface by averaging 10 scans at 2 cm^{-1} resolution. In late nymphs of *M. spinolai* (n = 3) at 24 °C with 40 % relative humidity using an ATR-FTIR spectrophotometer (Shimadzu, IRSpirit, Kyoto, Japan). Representative

spectra were selected from the recorded measurements to illustrate the characteristic peaks of each condition.

Thermogravimetric analysis of exuviae

The thermal degradation of exuviae samples was analyzed by thermogravimetric analysis (TGA; TA Instruments, model Q50). A sample of randomly recovered exuviae of covered nymphs in the laboratory colony, weighing between 8–10 mg was heated at a rate of 10 °C/min from room temperature to 800 °C under a constant purge-flow rate of nitrogen.

2.5. Chemical composition architecture of *M. spinolai* exoskeleton using confocal laser scanning microscopy

For specimen treatment, at least three transverse sections (~100 μm or less) were obtained from the dorsal abdominal cuticle of *M. spinolai* late nymphs (n = 3). Sections were rinsed three times in 75 % ethanol (5 s each) and mounted in glycerin (≥99 %, PhytoTech Laboratories) between a glass slide and a cover slip. Imaging was performed using a spectral confocal laser scanning microscope (Zeiss LSM 710, Carl Zeiss Microscopy, Jena, Germany) equipped with four solid-state lasers (405, 488, 543, and 633 nm) and used Z-stack imaging taking images at different zones of the specimens. For visualization, we used a 20x objective (Plan-Apochromat, numerical aperture e = 0.8). We then created maximum intensity projections using FIJI (ImageJ, National Institutes of Health, USA).

The autofluorescence of the cuticle was analyzed following the protocol of Michels and Gorb [46]. Accordingly: (I) soft endocuticle emits blue light when excited with the 405 nm laser and visualized using a bandpass filter transmitting 420–480 nm; (II) chitin non-sclerotized cuticle emits green light when excited with the 488 nm laser and visualized with a bandpass filter transmitting ≥ 490 nm; and (III) chitin sclerotized cuticle emits red light when excited with the 543 nm and 633 nm lasers and visualized with bandpass filters transmitting ≥ 560 nm and ≥ 640 nm, respectively. For image analysis, all channels were merged into an RGB by means of FIJI (ImageJ, National Institutes of Health, USA).

2.6. Scanning electron microscopy (SEM, FESEM)

General SEM imaging: The transversal cut samples were obtained by dipping nymph IV into liquid nitrogen to make a clean abdomen section with a razor blade. Nymphs and transversal cut samples were rinsed, fixed, and dehydrated following the protocol reported by Padilla-Manzano et al. [47]. For observations through Scanning Electron Microscopy (SEM), samples were coated with 10 nm Pt/Pd films by sputtering and then observed at different magnifications operating at 5 kV, using an Everhart–Thornley secondary electron detector (ETD) and working distances between 7–10 mm (SEM; ZEISS EVO MA10). For Field Emission Scanning Electron Microscopy (FESEM), samples were coated by sputtering with Au films of 5 nm thickness and then observed at different magnifications, operating at 10 kV, using an Everhart–Thornley secondary electron detector (ETD) and working distances between 7–10 mm (FESEM; FEI Quanta FEG250).

Thickness measurements: The thickness of the exocuticle of *M. spinolai* was measured directly from SEM images of the exuviae. Free edges revealed by the fracture of exuviae were oriented parallel to the scanning plane to prevent geometrical errors. The total cuticle thickness was obtained from SEM images of transversal cuts of the *M. spinolai* abdomen. Representative measurements of the thickness of the exocuticle at the abdomen, the legs, and other areas of interest are obtained by averaging about 40 data points taken at the desired representative area.

Indirect measurements of the thickness of the exocuticle of *M. spinolai* were achieved by directly measuring the thickness of exuviae taken in similar areas from SEM images. Free edges revealed by the fracture of exuviae were oriented parallel to the scanning plane to prevent geometrical errors. This procedure was applied mainly to exuviae taken from both the abdomen and the middle legs.

2.7. Atomic force measurements

Atomic force microscopy (AFM): Surface topographic characterization *M. spinolai* late nymphs was performed with a Witec Alpha 300 microscope equipped with AFM (tapping mode) to determine the geometrical features of the wrinkled surface of this insect. A 160 kHz resonance frequency cantilever was used (μmasch Hi Res-C14/Cr-Au), with tip radius 2 nm and stiffness k = 5 N/m. Overall, these choices allowed to reduction of adhesion during AFM image acquisition.

Young modulus measurements: All Young moduli were determined through AFM nano-micro indentation methods from the analysis of force curves in the compression stage (Fig. 1).

Soft endocuticle assessment: A diagram illustrating the process of indentation is shown in Fig. 1.a. Slides of about 100 μm thickness, obtained by transversal sections of the *M. spinolai* abdomen, are placed on a glass plate with the exocuticle oriented perpendicular to the plate. This preparation allows appropriate mechanical contact (flat) of the sample with the substrate. Force curves are interpreted through the Hertz contact formula as, $F = K\delta^{3/2}$, with $K = \frac{4}{3}E_s\sqrt{R}$, [48], which applies for deflections, δ, smaller than the cantilever tip radius, R, and where E_s is the Young modulus and ν the Poisson ratio; $\nu = 0.5$ is assumed. Here, diamond cantilevers of tip curvature radius R = 150 nm and stiffness 81 N/m (Nanosensors, Model: DT-NCHR-10) are used.

Hard exocuticle assessment: Regular cylindrical shells corresponding to leg exuviae and freshly extracted legs are used as samples for the assessment of exocuticle stiffness. These are first fixed to a glass slide through a double face adhesive, while an indenter deflects the shell perpendicular to the leg axis (Fig. 1b). A cantilever (Nanosensors, Model: DT-NCHR-10) provided with a diamond tip of curvature radius 150 nm is used. In this case, the force, F vs cylinder deflection, d, is modeled through, $F = 1.18E_t t^{5/2} d/r^{3/2}$, where E_t, t, and r are the Young

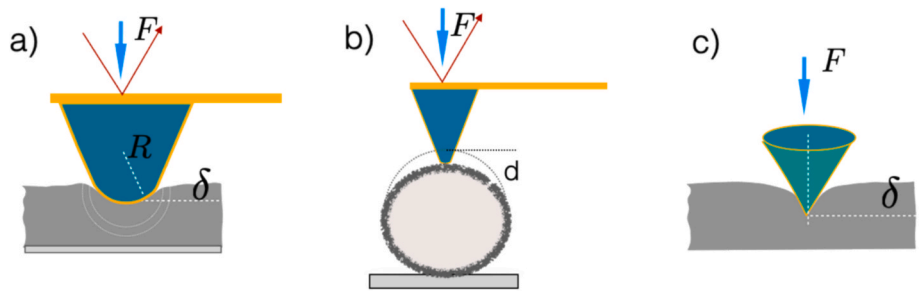

Fig. 1. a) Young's modulus assessment of soft endocuticle: diagram of the indentation of a cross section of the *M. spinolai* cuticle, oriented in a way that allows indentation of endocuticle, in the regime of penetration, δ≪ R (tip radius). Dashed circles indicating compression zones. b) Young's modulus assessment of hard exocuticle: Diagram of transversal indentation of a cylindrical sample. Legs exuviae and freshly removed legs are tested. c) Young's modulus assessment of the adhesive epicuticle: Diagram of compression with *conical indenter*.

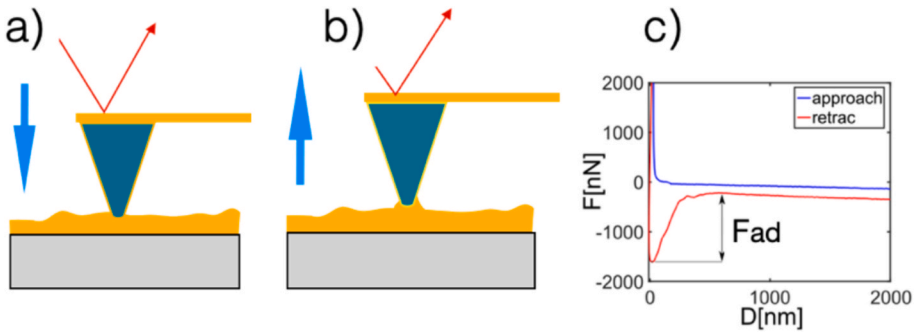

Fig. 2. Schema for adhesion assessment. a) Approaching of the tip to the sticky layer, b) and retraction. c) Typical approaching and retraction curves indicating the layer compression and the maximum force necessary (adhesion force F_{ad}) to detach the tip from the substrate, respectively.

modulus, the wall thickness, and the radius of the cylindrical shell, respectively [49].

Epicuticle assessment: The fit of the AFM force, F, vs the penetration, δ, allows for the assessment of the Young modulus of the adhesive layer. Because the thickness of the adhesive layer is only about a micron, relatively small indentations must be used which allows for the application of the Sneddon model [50], $F = \frac{2E_e tan(\alpha)}{\pi(1-\nu^2)}\delta^2$. Notice that the use of this model requires of deflections that must be much larger than the indenter radius R, i.e. $\delta \gg R$. Here E_e is the Young modulus of the soft epicuticle (sticky layer) and α is the semi-angle of the conical indenter (Fig. 1c). Notice that, in contrast to measurements in of endo and exocuticle, a SiNi RTESPR (Bruker) cantilever with a small tip radius, $R =$ 10 nm, is used to obtain force–deflection curves and fulfill the requirements of the Sneddon formula. Moreover, the cantilever has a semi-angle of 20°, and stiffness of 40 N/m.

Adhesion measurements: The adhesive property of wild and laboratory-reared *M. spinolai* late nymphs is evaluated through the acquisition of force curves in approaching and retraction (Fig. 2a and b) by measuring the adhesion force F_{ad}, which is directly determined by the magnitude of the force required to separate a semi-spherical tip from the sticky surface (Fig. 2c). Cantilevers SiNi RTESPR (Bruker) and ARROW-NC-10 (Nanoworld) of stiffness 40 N/m and tip radius of curvature 10 nm were selected. These provide consistent results because they are not polluted during the operation. In addition, due to its chemical nature, it effectively imitates the characteristics of dirt grains. The characterization of the adhesive force between the SiNi tip and the *M. spinolai* surface was achieved by means of a pico-force system (Veeco-IIIa), which provides sensitivity and manual control of tip-sample interaction. This control was suitable for identifying local flat areas of the *M. spinolai* adhesive surface for optimal positioning of the AFM-tip. For the assessment of viscous contribution, the tip speed (approaching and retraction) is varied in the range between 0.14 μm/s and 35.0 μm/s. To obtain a representative number of *M. spinolai* force curves, after collecting a force curve, the tip is moved about 400 nm following a 10x10 squared matrix to a new test point, where a new force curve is taken. This process allowed us to obtain enough data points as required to estimate the average of the adhesion force, $\langle F_{ad} \rangle$.

2.8. Morphology and Topography mathematical analysis

The analysis of the mathematical properties of the wrinkled surface was performed by calculating the "Gaussian curvature," i.e., the product of the principal curvatures of the *M. spinolai* surface, obtained through AFM profiles. To characterize the degree of flatness of the wrinkled nymph surface, the Gaussian curvature calculation was implemented numerically and applied to the topographic AFM surface profile. Our code is written in MATLAB and basically selects a subarea of the surface, whose size is much smaller than the wrinkles size, performs a noise filtering process, adjusts the surface with a smooth function, and then estimates the principal curvatures of the subarea (see Supplementary Information for details). The process leads to a representative Gaussian curvature field in a selected zone of size containing several wavelengths.

3. Results

As stated, *M. spinolai* is a sylvatic species living in arid and semi-arid ecosystems, unlike other Triatominae species *M. spinolai* are active during daytime, these specific conditions allow specific adaptations to appear due to selective pressure because of adverse and unpredictable environmental conditions [28,30]. In the present study, we provide insights into the material that allows *M. spinolai* to be a successful diurnal bloodsucker, its exoskeleton (Fig. 3). It presents camouflage behavior in all nymph instars, actively covering in dirt grains which remain attached to the epicuticle on the insect surface (Fig. 3a). Also, we studied the cuticular abdominal expansion, an example of the extraordinary geometrical change due to the abdominal expansion, resulting in an almost ellipsoidal shape after the feeding process, is shown in Fig. 3b This abdominal expansion is suggested to occur by means of a mechanical strategy employing hierarchical layered and microstructured highly stretchable material consisting of a thin exocuticle and a thick endocuticle (Fig. 3c).

Relative weight increase. How much can it withstand?

We analyzed samples of late nymphs (IV and V, n=60 each) relative weight increase. Detailed information about ranges and the means of weight increase through the engorgement process is shown in Table S1. This capacity, along with abdominal expansion, must be accompanied by a highly elongational property of the cuticle.

Chemical profile and design of the *M. spinolai* cuticle

The ATR-FTIR spectra acquired on the dorsal cuticle of *M. spinolai* nymphs (Fig. S1a) were used to suggest the composition of the exoskeleton and the soil grains adhered to their surface. Late nymph cuticle spectra showed characteristic bands of chitin and associated proteins, while spectra from dirt-covered nymphs revealed additional signals consistent with silicate minerals from the attached particles. Thermogravimetric analysis of *M. spinolai* exuviae (Fig. S1b) revealed three distinct mass-loss regimes followed by a residual fraction. The remaining mass at 800 °C indicated a significant proportion of non-decomposable material in the cuticle and attached to the surface.

Confocal Laser Scanning Microscopy allowed us to visualize hierarchical design based on the distribution of cuticular elastic proteins (such as resilin), non-sclerotized chitin, and sclerotized chitin based on each respective autofluorescence (see Section 2.5). The abdominal cuticle section is shown in Fig. 3d, two different evident zones are present, a large endocuticle emitting mainly blue and green autofluorescence, and a thin red layer on top forming microstructures of wrinkles and pillars. Also, a few yellow zones are seen in transition zones (green and a little red overlayed).

Topography and folding understanding: The stretchable *M. spinolai* cuticle cuticle

The *M. spinolai* hierarchical structure presented (Fig. 3e), related to

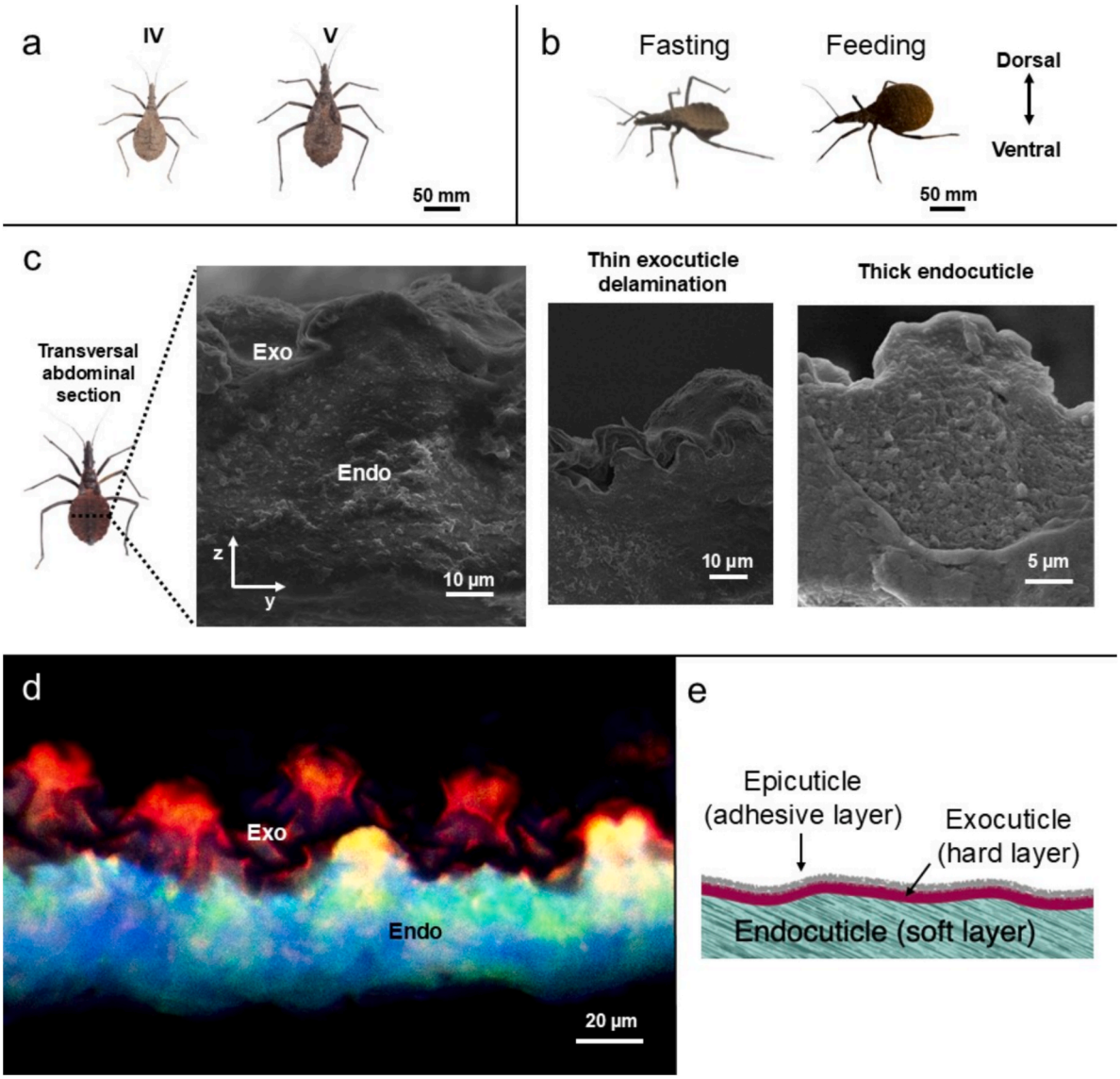

Fig. 3. *M. spinolai* exoskeleton features and hierarchical design. a) Late nymphs IV and V of *M. spinolai are* both camouflaged by epicuticle-adhered dirt grains. b) Late nymph abdominal expansion after feeding. c) Transversal abdominal section FESEM micrograph showing layers: Exo (exocuticle), a thin layer and its delamination; Endo (endocuticle), a thicker and more compliant inner layer. d) CLSM of abdominal dorsal cuticle showing a hierarchical material gradient with differential autofluorescence. e) Schematic representation of specimens cuticular design.

the abdominal cuticle (Fig. 4a) mechanical performance. Two types of structures with remarkable elongational properties were observed, namely, a dense pattern of wrinkles and a network of pillars distributed in a close and nearly hexagonal network (Figs. 4b and 4c). SEM images of a transversal section of the cuticle revealed an exterior stiffer thin layer (exocuticle), which protects a soft and highly stretchable inner polymeric composite (endocuticle) (Fig. 4d). The amplitude of the wrinkled structure could be directly seen in Fig. 4d (white line), from which the real surface of the cuticle was estimated. Indeed, by means of edge detection and integration of the resulting profile curve, the length (in white) of the segment was obtained, which was approximately 40 % longer than its apparent length (in red), and from there, an estimate of the available exocuticle surface area by wrinkles of factor 2 is obtained. Regarding the volume capacity of *M. spinolai*, assuming an ellipsoidal shape for its abdomen, a factor of 6 of volume enhancement is obtained. Additional quantification of the great capacity of *M. spinolai* cuticle to elongate was obtained by comparing its state before and after feeding. Fig. S2 shows two individuals at the same stage of growth. Pillar's separation is regular; on average, this distance is 37 µm and 58 µm, before and after feeding, respectively. If S is the surface of the extended surface (almost unwrinkled), relative extensions in both directions lead to a surface change with respect to the apparent surface, S_{app} (wrinkled) of $\Delta S/S_{app} = (S - S_{app})/S_{app} \approx 1.6$, which was, as expected, smaller than the maximum capacity of wrinkles to elongate, as previously obtained (factor 2). The pillar's mechanism of cuticle storage is not straightforward, and the pillar function is not completely elucidated through the mechanical approach presented here. However, a rough estimate of the excess surface stored in pillars was obtained by measuring the area included in the pillar mantle. Using the definitions in Fig. S3, the excess surface, ΔSp, is, $\Delta Sp/\pi R^2 = [(R+H)^2 - R^2]/R^2 = [H^2 + 2RH]/R^2$, where $H \simeq 10$ µm is the typical height and $R \simeq 12$ µm is the typical radius of pillars, $\Delta Sp/\pi R^2 \simeq 2.3$, indicating that each pillar stores about 2 times the pillar's apparent surface (πR^2). Thus, in the non-pulled condition, although wrinkles in the pillars are nearly orthogonal to the surface, these stored about the same surface as horizontal wrinkles per unit of apparent area (factor 2). Of note, this result indicates homogeneous surface availability, a condition that is necessary to prevent stress concentration and to allow homogenous exocuticle elongation.

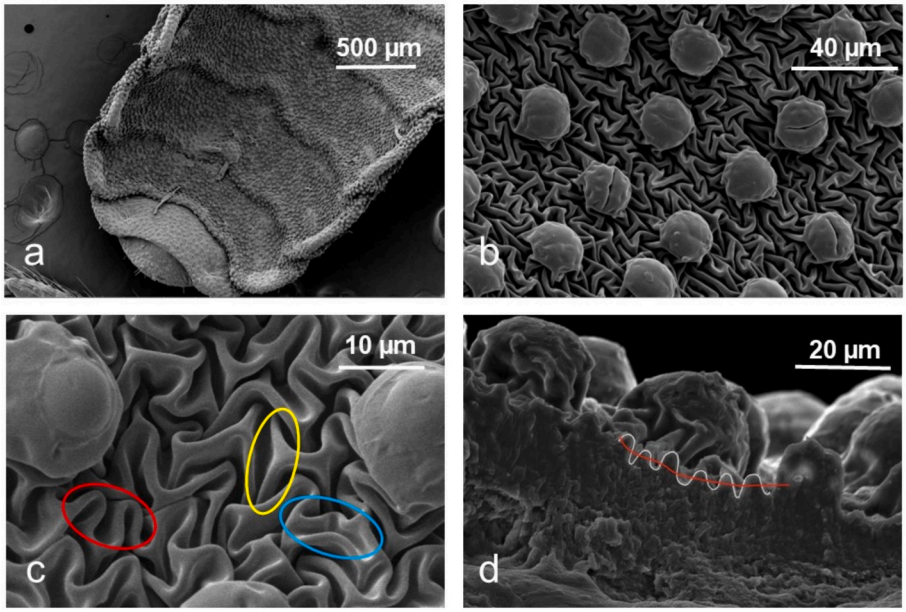

Fig. 4. SEM and FESEM images of the cuticle structure of starving late nymphs *M. spinolai* at distinct magnifications. a) Dorsal view of abdominal section in late nymph *M. spinolai,* showing large-scale structures. b) Wrinkles and pillars observed in a nearly compact hexagonal packing small scale. c) Magnification details of the cuticle in abdominal section, depicting a dense network of wrinkles. d) Cross-section of the cuticle in late nymph revealing the presence of the structured wrinkle pattern of a characteristic size (white line); red line represents the apparent length of cuticle segment.

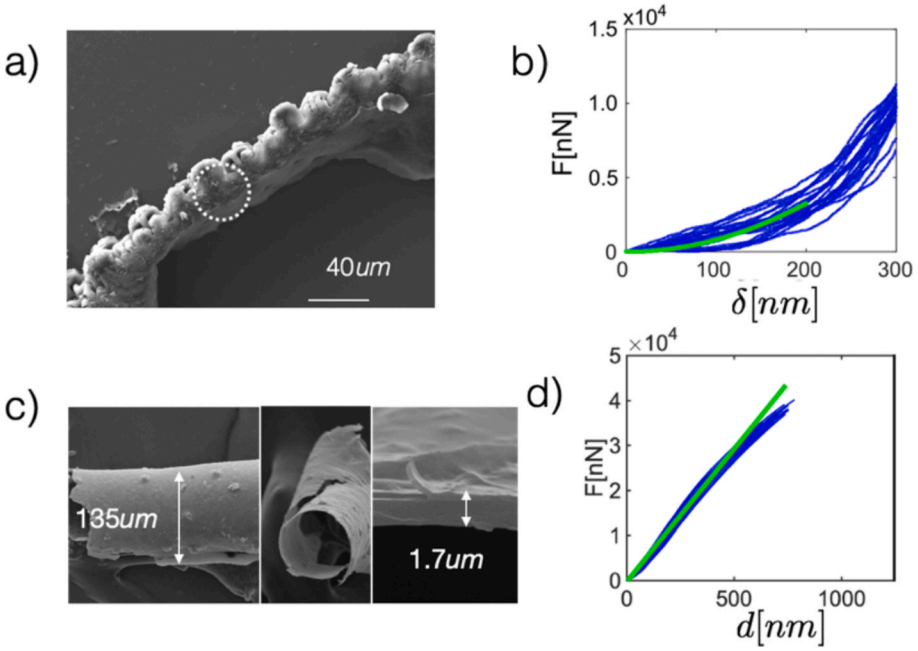

Fig. 5. a) A cross-section of the *M. spinolai* cuticle, oriented in a way that only allows indentation of soft endocuticle. The dashed circle indicates indentation zones. b) Typical force curves and best fit (green) to data using the Hertz formula. c) SEM images of a cylindrical leg from exuviae tested perpendicular to its axis. Left: side view; middle: top view; right: amplified top view indicating wall thickness. d) Typical force curves and best fit (green).

Mechanical properties of *M. spinolais* exoskeleton: Young's modulus and adhesion

AFM indentation on transversal stripes taken at the abdomen of *M. spinolai* (Fig. 5a), located on a rigid glass support, made it possible to determine the Young modulus of soft endocuticle. In this case, the AFM force curves (Fig. 5b) were analyzed (See Methods Section), leading to $E_s \simeq (100 \pm 30)$MPa. More than forty force curves were averaged. Fresh cut endocuticle, and 4 hr and 24 hr. dried at ambient conditions exocuticle, where assessed without significant changes in the elastic modulus. Therefore, we concluded that Young's modulus is not significantly affected by drying, at the conditions explored. However, soft endocuticle becomes increasingly brittle for further drying.

Fig. 5c depicts SEM images of a nearly cylindrical shell of exuviae of diameter close to 135 µm, and whose average thickness is about 1.7 µm. The force vs. displacement curves, obtained through indentation (see method section) is depicted in Fig. 5d. Fitting the average force curve, using as input the thickness of cylindrical samples ($t \approx 1.7$ µm), leads to, $E_t \simeq (8 \pm 2)$ GPa. This value was about 80 times higher than that of the

M. spinolai endocuticle. To check if the Young's modulus of exuviae accurately reflects the properties of exocuticle, additional measurements of Young's modulus of fresh cylindrical legs were performed, following the same procedure as above. The obtained values were about 30 % lower than those captured in exuviae, which cannot be attributed to the stiffness contribution of the soft inner part of the leg. However, this is due to an overestimation of the exocuticle thickness. Additional measurements aimed at assessing the variability associated with sample heterogeneity is given in Fig. S5. For instance, although nearly cylindrical, legs are not homogeneous in thickness, and their mechanical properties may vary at distinct zones. This has been controlled by collecting series of force curves along the main axis of exuviae and legs. These explorations revealed a modulus variance of the order of 30 %. In addition, a comparative table using samples at distinct conditions is given in Supplementary Information (Table S2).

Wrinkles and pillars formation scenario

In *M. spinolai*, one possible scenario for the wrinkled pattern formation is the following: i) Extremely high cuticle stretching during feeding. ii) Delamination of the cuticle if stretching exceeds a threshold, leading to cuticle fracture and delamination [51,52]. Thus, exocuticle remodeling leads to a significant increase in the exocuticle area in *M. spinolai*. iii) As the stored food is consumed, the abdomen volume decreases, and a network of wrinkles develop due to exocuticle buckling. iv) The cuticle pattern is first a network of parallel wrinkles as it would be in uniaxial compression. However, due to the biaxial character of the tension relaxation of the soft substrate –resulting in a biaxial compression of the layer– a zigzag secondary structure develops on parallel wrinkles (Fig. 4c; red circle), which is known as the Herringbone pattern [53,54]. Such a structure can be very regular, as seen in previous works [53]. However, in the case of *M. spinolai*, due to the dramatic change in area, the structure becomes more complex and exhibits a prominent feature corresponding to a zigzag structure, composed of high amplitude wrinkles, folded perpendicular to the wrinkle longitudinal axis (Fig. 4c: red, blue, and yellow circles). On the same line, pillars exhibit a complex fold structure. Despite this complexity, cuticle pulling induced through feeding indicates that the wrinkles in a pillar are organized in a similar manner to wrinkles in a round tablecloth (see Fig. S3). This suggests that pillars are formed through a dramatic process of compression of a flat cuticle, thus causing the top part of the pillars to become more rigid. In any case, pillars provide an additional mechanism to store excess surface. The pillar's origin and the dynamic process that leads to pillar formation have not been elucidated yet. Here, we propose that pillars are formed because of a secondary instability that ejects collapsed wrinkle zones (which are more rigid) out of the average plane; this expulsion would be responsible for the creation of the relatively flat circular zone where the pillars are located. This scenario was inspired by the observations in Fig. 6a, which shows highly compacted, flat zones, likely of enhanced rigidity, coexisting with well-developed pillars. Of note, some well-developed pillars at the interface of collapsed wrinkles were close together, suggesting that an advection of pillars took place to generate a structure with nearly homogeneous spacing between the pillars. An incipient pillar made of four collapsed wrinkle structures is shown in Fig. 6b. Fig. 6c shows a different zone where both wrinkles and incipient pillars coexist with developed pillars. Small amplitude wrinkles at the top of pillars and a large fold (Fig. 6d) both imply that all areas were subjected to compression-inducing buckling of the cuticle. It is worth mentioning that a wrinkles-to-folds transition has been observed in highly compressed, initially flat films adhered on a soft substrate [54], which suggests that pillars may result from the folding instability of a wrinkled pattern. However, in a system of infinite thickness, folds penetrate as compression increases [54]. In contrast, due to the finite thickness effects in *M. spinolai* exoskeleton, we expected that high-amplitude folds would be ejected instead, which would result in pillar formation.

Wrinkles

Wrinkle formation is a ubiquitous phenomenon resulting from the buckling of a thin, rigid layer adhered to a soft substrate [55]. Indeed, if compression is applied along the plane of the layer, due to the relatively high elastic energy cost of compression, bending is more advantageous, producing out-of-plane exploration of the layer leading to a nearly periodic structure of wrinkles, whose size is selected according to: $\lambda = 2\pi(3B/E_s)^{1/3}$ [55], where $B = E_t t^3/[12(1-\nu^2)]$ is the bending stiffness of the rigid layer (exocuticle) of thickness t, Young modulus E_t and Poisson ratio ν, and E_s is the Young modulus of the soft substrate (the endocuticle). B accounts for the energy involved in changes of curvature of the elastic exocuticle. Thus, at onset of wrinkle formation, both the exocuticle bending, and the endocuticle elastic deformation energies are minimized as accounted by the previous formula. To check whether the

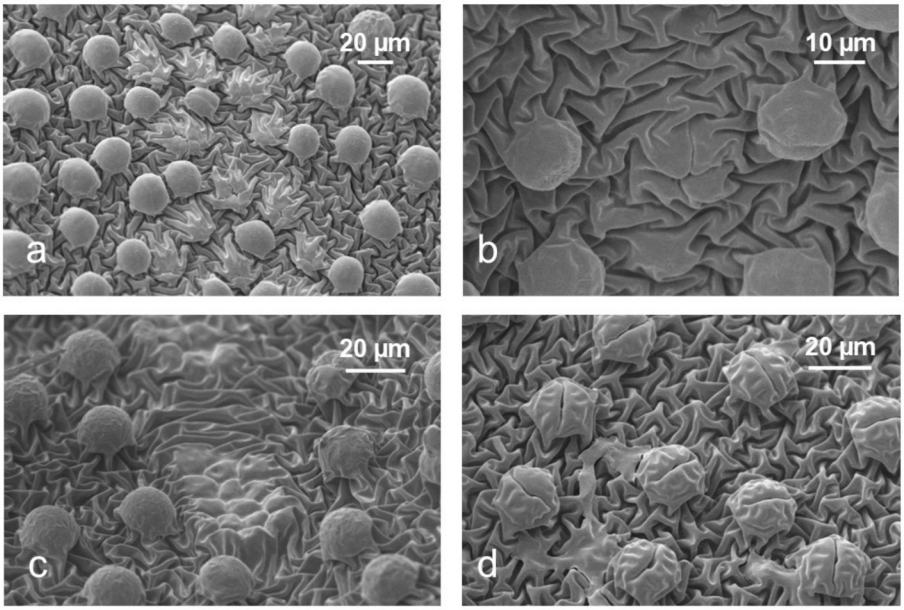

Fig. 6. Sections of late nymphs *M. spinolai* dorsal exocuticle showing pillar formation. a) Coexistence of well-developed pillars and highly packed precursor structures. b) Close-up of an incipient pillar made of four collapsed wrinkle structures. c) Apparent source of pillars (middle). d) Top of pillars presenting wrinkles and a fold.

elastic instability scenario captured the features of the *M. spinolai* exocuticle, transversal cuts were observed under SEM, revealing a total cuticle thickness ranging from 12 μm to 50 μm, while the wavelength at onset varied from 10 μm to 15 μm, respectively, depending on the abdomen zone (Fig. 4d). The exocuticle was indeed much stiffer ($E_t \simeq (8 \pm 2)$ GPa) than the endocuticle ($E_s \simeq (100 \pm 30)$ MPa). With these values and taken the average thickness of the exuviae in the dorsal region, $< t > \simeq 1$ μm, we estimate the wrinkles wavelength [55] , $\lambda \simeq 16 \pm 4$ μm. This value is of the order of the wrinkle's wavelength pattern observed at vanishing wrinkle amplitude on the exocuticle. Thus, the principle of energy minimization of elastic energy captures well the typical size of the wrinkled structure, suggesting that the pattern observed in *M. spinolai* exocuticle arises mainly from a mechanical instability of the stratified exoskeleton.

Epicuticle properties

Elastic properties: To estimate the elastic and viscous components of the sticky epicuticle, we registered forces curves in a wide range of approaching and retracting speeds on the epicuticle. The typical elastic modulus obtained from the fit of compression curves (Fig. 7a), $E_b = (3.5 \pm 1)$ MPa, indicates that the adhesive epicuticle is relatively soft (See Methods).

Viscous effects: These effects were estimated by calculating the size of hysteresis cycles. Indeed, we performed a loading–unloading cycle (Fig. 7b) and evaluated the dissipated energy U_D over a cycle as the area of the resulting hysteresis curve in the positive quadrant. The ratio between the dissipated energy and the total energy, U_D/U_T, provides a measure of the amount of viscous dissipation with respect to the elastic energy and establishes the importance of the viscous effect. We found that U_D/U_T (Fig. 7c) slowly increased with speed. We conclude that viscoelasticity does not significantly increase the adherence capacity of the adhesive material. This result is consistent with the fact that grains remain adhered to the *M. spinolai* surface without being removed for a long period of time, indicating that the adhesive layer does not significantly flow.

The adhesive property of M. spinolai nymphs: The form of the retraction curve indicates the existence of adhesion because a maximum pulling force, F_{ad}, is necessary to detach the cantilever tip from the surface. Since the approaching curves and analysis revealed (Fig. 7a) that the adhesive epicuticle is made of a soft material, we employ the Johnson − Kendall − Roberts (JKR) formula [56], which relates the work of adhesion [energy/per unit area] to the adhesion force as: $W_{ad} = 2F_{ad}/3\pi R$, where R is the tip radius of curvature. The high variability of the adhesion force is evidenced in Fig. 7d, probably due to the scarcity of flat areas on the wavy cuticle of *M. spinolai* and the variability of the thickness of the epicuticle. Histograms of the W_{ad} show a wide variability in this parameter (Fig. 7e). However, we noticed that the whole exoskeleton was covered by grains (Fig. 8a), and legs presented smoother surfaces due to the absence of wrinkling. Despite these topological differences, adhesion values did not present dramatic changes, indicating that microstructures on the cuticle did not significantly hamper adhesion measurements. To check whether the tip was not polluted by the sticky material covering the *M. spinolai* cuticle, we verified that it did not adhere to a clean glass surface (control) prior to and after capturing a set of force curves. Using the JKR formula and the typical values of $< F_{ad} >$, we find that $W_{ad} = (10 \pm 3) J/m^2$, indicating that adhesion was likely due to van der Waals molecular forces [48]. In addition, there was a relatively low effect of the adhesion force on the retracting speed over two decades (Fig. 7c). Thus, the performance of the sticky substance on the *M. spinolai* exoskeleton may rely on the capacity of this material to deform, allowing surface contact with irregular grain surfaces, especially at low deformation rates.

Although *M. spinolai* glue is weak (10–20 Pa), compared to commercial adhesives (1–10 MPa), the observed adhesion energy is enough to bond dirt grains. Indeed, SEM images demonstrated that the size, R_g, of the grains adhered to the back of *M. spinolai* varied in size, ranging from 20 μm to 200 μm (Fig. 8b) and that the adhesion points exhibited a variety of sizes, from 1 μm to 3 μm (Fig. 8c-d).

4. Discussion

Arthropods are characterized by the presence of an exoskeleton. Below, we discuss the composition, properties, and mechanisms behind this biological material as an example of how it relates to *M. spinolai* habits when coping with a hostile environment.

Weight increase after feeding

We compare the weight gains of two late nymphs (Table S1). There is a gap of 80 % in the mean between nymph IV and V, we relate this increase with physiological preparation for its last metamorphosis to adult stage, process that requires the development of new structures and organs in Triatominae, such as fully developed genitalia and wings for

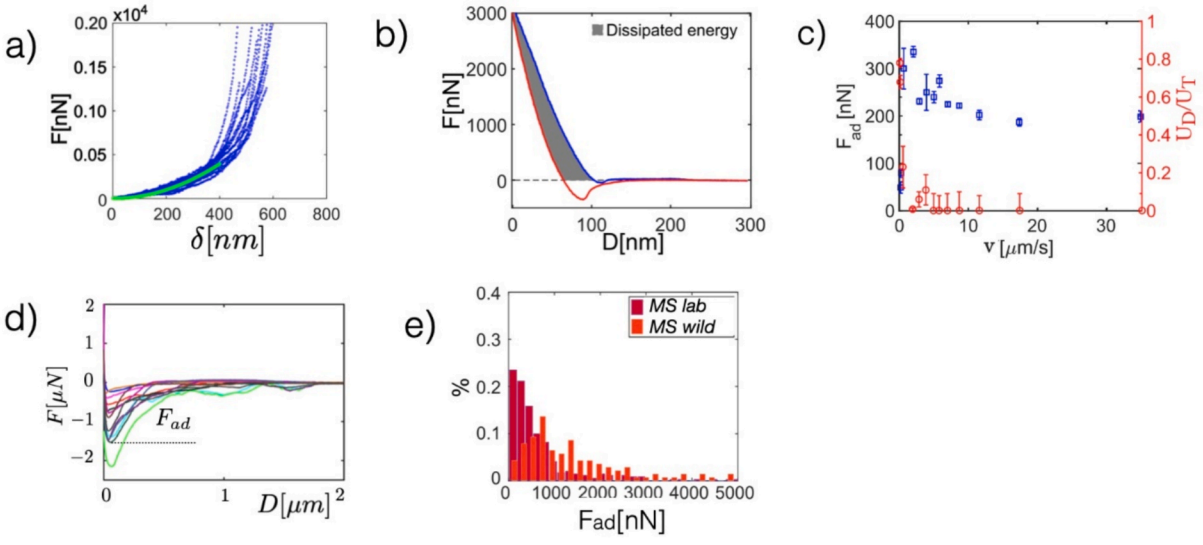

Fig. 7. a) typical compression curves for the assessment of young's modulus of the adhesive epicuticle. the green line is the best fit to the data using sneddon's formula. b) approaching (blue) and retraction (red) force curves at low amplitude indicate adhesion and hysteresis (dissipated energy) due to the viscous effect, ud (area in gray). c) ratio of dissipated energy to the total energy, U_D/U_T (red) and force adhesion F_{ad} (blue) as a function of the retraction speed. d) Typical force vs displacement curves in retraction, illustrating the variability of adhesion force, F_{ad}. e) Histograms of F_{ad} for wild and laboratory-reared *M. spinolai*.

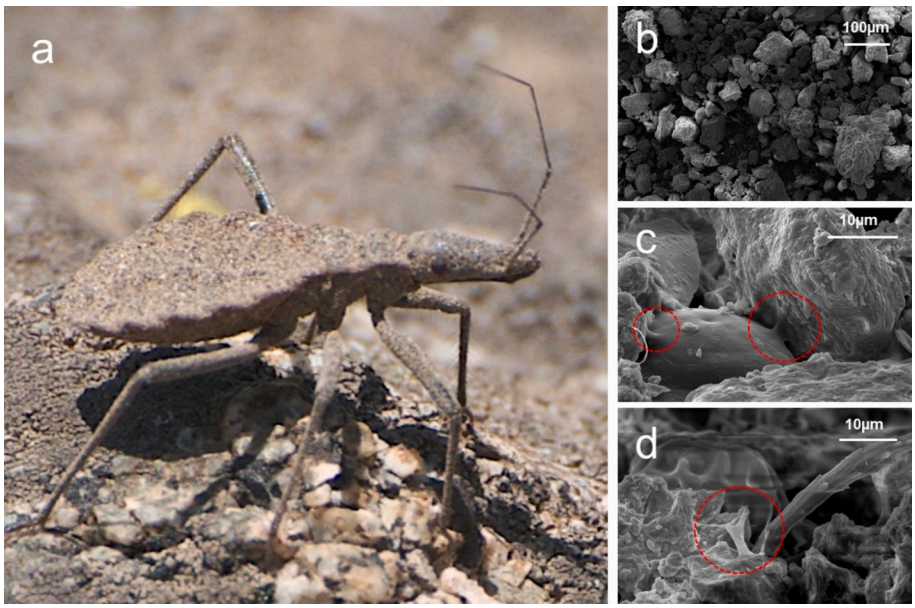

Fig. 8. Dirt adhesion in *M. spinolai*. a) *M. spinolai* wild nymph covered by dirt grains. b) SEM image showing typical dirt grain distribution on the *M. spinolai* cuticle. c) SEM image depicting adhesion points near the pillar top (encircled). d) SEM image of extended filaments (encircled).

adult stage dispersal and reproduction [26]. The nutritional requirements of adult insects are closely tied to their reproductive processes. Many authors have shown that female blood-sucking insects have reproductive batches of eggs after each blood meal; this correlation has been called gonotrophic concordance, where the quantity of eggs is proportional to the meal size with a limit based on the number of ovarioles available [57]. This has been studied in Triatominae; for instance, Nattero et al. (2011) used two different blood sources to feed the *Triatoma infestans* kissing bug, the *Cavia porcellus* rodent, and the *Columba livia* bird, to evaluate the effect of blood meal quality and quantity on reproductive parameters such as fecundity (number of eggs). The findings of this study indicated that there is a positive correlation between fecundity and larger meals, regardless of the meal source[58]. An experiment was carried out in *Triatoma patagonia* before establishing a tendency like the one we found [59], meaning that increasing the meal size leads to reproductive benefits for the insect.

Chemical design of *M. spinolai* cuticle

Several studies have reported chemical composition and design of exoskeletons in arthropods [9,11,14,18,20,21,60]. Chitin, a polysaccharide of N-acetylglucosamine, is one of the main components of insect cuticle. Chitin presence has been confirmed through extraction and characterization using ATR-FTIR in an exhaustive study reported by Sharbidre et al. for *Coridius nepalensis* (Hemiptera: Dinidoridae), establishing a similar signal assignment as we did for Amide stretching, –OH stretching, and C-H acetyl stretching [60]. On the other hand, this chitin presence has been analyzed in other arthropod groups through other characterizations, such as Raman spectroscopy presented by Amini et al. (2018) for *Alpheidae* specimens [11]. In nymphs covered with a thin film of dirt-grains this feature adds an extra difficulty performing non-invasive analysis; in our work, we showed the presence of a wide band around 1017 cm^{-1}, according to this we suggest it could be related to the chemical composition of the soil adhered to the insect, allowing us to choose a similar instrumentation material to perform adhesion measurements with AFM. Previous studies on the mineral composition of soil accuse the presence of a band around 1000 ~ 1100 cm^{-1} due to the presence of silicates [61]. In Chile, studies regarding the composition of different soil samples were performed by Ramírez et al. (2020) with FTIR spectroscopy, assigning the same Si-O stretching mode in semi-arid soil samples, as in our case [62].

Our findings also suggest that there is a protein part of the material seen as a wide band around the Amide I region; this phenomenon was studied before by FTIR and Raman spectroscopy by Harris & Chapman (1995) [63]. "Soft"-cuticle proteins and their secondary structure were studied in the giant silk moth *Hyalophora cecropia* (Lepidoptera: Saturniidae), which showed similar bands to the ones we detected [64]. The protein presence in insect exoskeletons plays a significant role in the modulation of mechanical properties in chitin-protein composites [65]. As an example in insects, sclerotization is the sclerotin-chitin cross-linking process by covalent bonding, and it plays a fundamental role in the mechanical performance of the cuticle and its functionality [19–22,66,67].

Thermogram analysis of *M. spinolai* exuviae was performed and analyzed by assigning different mass loss regimes to the chemical composition of the exuviae material (Fig. S1b). The first regime was associated with 9,8% water evaporation from the material (Regime 1). We established a 34.0 % regime until 450 °C (Regime 2) associated with chitin and non-cross-linked proteins. And later we defined a regime of constant mass loss between 450–800 °C (Regime 3) associated with sclerotized cuticle and possibly inorganic compounds present in the composite. In comparison, a study performed by Rong et al. in the oriental fruit fly *Bactrocera dorsalis* Hendel (Diptera: Tephritidae) cuticle assigned an organic degradation regime of chitin and proteins between 260 °C and 620 °C. Then, they considered an inorganic mineral part regime until 850 °C associated with the amorphous calcium phosphate and contrasted with Differential Scanning Calorimetry, observing a characteristic peak of its exothermic crystallization [68].

As stated, proteins play a crucial role in modulating the mechanical properties of the insect cuticle, therefore studying the hierarchical distribution of these proteins and their mechanical properties is fundamental for better understanding on how using conservated material blocks nature has come with unique mechanical strategies according to functionality [46,65,69]. A well-known example is resilin, a highly elastic protein that has been shown to modulate interfacial and physical phenomena [70], playing a fundamental role in structures related to mechanical support, flight, and reproduction, where elasticity is functionally required [69,71–73]. In contrast, sclerotin plays a central role in the process of sclerotization, during which cuticular proteins cross-link with chitin through oxidation and polymerization reactions due to phenolic compounds incorporation, resulting in the progressive coloring and hardening of the cuticle and increased rigidity and resistance

[74,75]. Due to their autofluorescence, the distribution of key proteins, chitin and it's sclerotization can be characterized using the Michael and Gorb confocal laser scanning microscopy methodology [46]. This methodology allows the identification of the diverse chemical architectures and hierarchical structural design for specific functions related to unique biological adaptations [46,69]. This chemical and structural characterization can be complemented with nano-indentation techniques, allowing to propose a correlation between materials architecture and mechanical strategies [20,21,67,72]. For example, the elastic properties of the desert locust *Schistocerca gregaria* (Orthoptera: Acrididae) femora and hind femora exoskeleton were analyzed before considering the sclerotization level of the material and its mechanical performance such as elastic modulus. These studies concluded that sclerotization plays a major role in increasing the elastic modulus of the material microstructures, in accordance with the insect habits and mechanical stress resistance requirements for functional design [20,21,67]. Same has been performed to explain adhesion strategies in *Coccinella septempunctata* (Coleoptera: Coccinilidae) showing a material gradient in tarsal cuticle and relating the chemical gradient with the mechanical performance in different zones [18]. Most recently, this technique has been used to relate the morphology, material composition, and mechanical properties in raptorial forelegs of two praying mantises having different prey preferences *Sphodromantis lineola* and *Gongylus gongylodes* (Mantodea: Mantidae). Here, they present evidence on material gradient composition and mechanical properties related with prey preference and complementing chemical composition with energy-dispersive X-ray spectroscopy (EDX) elemental analysis [22]. Although CLSM autofluorescence provides valuable qualitative information on the relative distribution of soft proteinaceous cuticle, non-sclerotized and sclerotized cuticle, other proteins could have the same excitation-emission spectra as resilin [22,69]. The determination of individual components would require complementary analyses, such as immunolabeling or proteomic approaches [69]. Nonetheless, the observed blue-emitting regions are consistent with areas typically enriched in resilin—a protein known to store elastic energy and to support repeated deformation–recovery cycles in biological structures [69]. Thus, our autofluorescence-based interpretation is suggested to be aligned with the known functional roles of resilin in insect cuticles[22,46,69].

As shown, *M. spinolai's* exoskeleton is a chemically hierarchical material. Exocuticle presents as a chitin sclerotized thin layer showing red emission and is also present in surface microstructures of pillars and wrinkles (Fig. 3d). Endocuticle is shown to be blue due to autofluorescence emission of cuticular proteins such as resilin. Non-sclerotized chitin is also present as a green autofluorescence. There is also a yellow zone present (mix of green and some red), and previous studies have already reported a transient material between the endo and exocuticle called mesocuticle [14,67].

Altogether, the chemical architecture in a hierarchical layer structure (Fig. 3d) is fundamental on understanding elongational physical strategies and their suggested mechanism of formation. As a sclerotized material, exocuticle is stiff and brittle but easy to bend, which leads to a micro-structuration process facilitated by a soft-compliant endocuticle. As a result, there is a pattern of wrinkles and pillars that act as exocuticle reservoirs, as we delve into below.

Mechanics and micro structuration in the *M. spinolai* cuticle

Although methods for the assessment of mechanical properties of thin films are scarce and difficult to apply, the Young's modulus of the *M. spinolai* exocuticle and soft endocuticle were obtained through nano-indentation methods. The exocuticle's wrinkles and the strong coupling to the soft endocuticle pose two major challenges. These issues greatly hinder both the determination of the load point and the development of realistic physical models that account for this coupling and from which mechanical parameters may be deduced. Therefore, an alternative approach was explored by testing the exuviae free of soft membrane instead of the composed cuticle. On the one hand, although most exuviae are irregular and wrinkled, it was noted that the exuviae leg is more uniform in structure; it has a well-defined cylindrical shape with a relatively constant wall thickness, which makes it easier to model the mechanical response of the exuviae leg when subjected to indentation. On the other hand, partial assessment of the soft component was achieved by indenting transversal cuts of the *M. spinolai* composite layer. Overall, this approach enabled the mechanical characterization of the structured cuticle.

The elasticity of the exocuticle: Using the indentation methodology, the average value of the elastic modulus of the hard film resulted in $< E_t > \simeq 8$ GPa. This value seemed too high compared with that of Chitin [76], which is about 300 MPa. However, as demonstrated by Li et al. [21], a similar value for the elastic constant was found in the hind femora of desert locusts, likely due to a high degree of sclerotization, as evidenced through confocal fluorescence microscopy [21]. According to our results, a comparable level of sclerotization was observed by CLSM for the *M. spinolai* exocuticle emitting red autofluorescence.

Elasticity of soft endocuticle**:** Transversal cuts of the *M. spinolai* cuticle provided suitable samples for the mechanical assessment of soft endocuticle through nanoindentation. The observed value was $< E_s > \simeq$ 100 MPa, which is like the chitin Young modulus [76], in agreement with the chitin content in the cuticle, as suggested in our ATR-FTIR analysis and complemented with CLSM for the elastic protein and non-sclerotized chitinous endocuticle visualization.

Wrinkles: The measurement of the endocuticle and exocuticle Young modulus, along with the principle of energy minimization of elastic energy, effectively capture the typical size of the structure, which in this case is about 12 μm, suggesting that the wrinkle pattern observed in the *M. spinolai* cuticle has a mechanical origin. This was also supported by the fact that the Gaussian curvature [77] was almost zero in typical wrinkled zones, as demonstrated in SI (see Fig. S4). This result indicates that the wrinkled structure can be flattened to a plane. Although it was not possible to verify whether a pillar can be flattened to a plane (zero Gaussian curvature) during this investigation, the organization of the wrinkles and folds in pillars, like a tablecloth, suggests that this would be the case. In addition, pillars and wrinkles store about the same relative area, indicating that the excess surface is evenly distributed throughout the exocuticle. Moreover, the wrinkle pattern in the *M. spinolai* cuticle exhibited similar complexity and features to those observed in the Herringbone pattern in purely mechanically stressed systems [78], suggesting that cellular growth does not affect the *M. spinolai* wrinkle structures.

Adhesion: The typical forces sustained by filaments and bridges are valuable information to estimate the mechanical resistance of the "granular exoskeleton". We assumed that the glue could fail either due to the detachment of adhesive points or stretching at a given yield stress σ y, which characterizes filament development and its failure. First, since the observed adhesive points were about $l \approx 3$ μm in diameter (red circles in Fig. 8c-b), the force necessary to achieve detachment, F_d, was estimated as $F_d \approx \pi l^3 E_b / R_c$, where R_c is the typical radius of curvature at the contact, $R_c \sim 10$ μm and $E_b \approx 3$ MPa, the elastic modulus of the adhesive. Thus, $F_d \approx 10$ μN, which would allow it to sustain a maximum weight equivalent to a grain with a size of about $R_g \approx 300$ μm, which is consistent with the larger grains observed on *M. spinolai* (Fig. 8a), (obtained from $F_d \approx 4/3\pi\rho g {R_g}^3$, where ρ and g correspond to the grain density and the acceleration of gravity, respectively). Second, assuming that the yield stress is about ten times the Young modulus, $\sigma_Y \simeq 30$ MPa, as in rubber-based materials, and that σ_Y provides the force at yielding, F_Y, as, $F_Y \simeq \sigma_Y \pi \varrho^2$, where ϱ is the radius of the filament. The question is, what would be the filament radius, ϱ, able to sustain a dirt grain with a size of about $R_g \simeq 50$ μm. This is given by $4/3\pi\rho g {R_g}^3 = \sigma_Y \pi \varrho^2$, leading to a ϱ value of approximately 15 nm, which is slightly smaller than the size of the observed filaments of about 100 nm, but it is consistent with the adhesion of larger grains observed in *M. spinolai*. Fig. 8c) and d) suggest that *M. spinolai* utilizes a combined strategy where pillars offer both efficient sticky points (flatter than wrinkles) and obstacles to prevent

grains from rolling. In addition, under some circumstances, sticky bridges between neighboring grains and long filaments that surround grains may be developed (Fig. 8d). These structures confer some additional integrity to the granular layer.

Overall, adhesive assays indicated that the adhesion energy was sufficient to sustain the typical grain size carried by the insect, which is around 100 μm, preventing the adhesion of larger grains or debris that may negatively affect *M. spinolai* displacement, and providing easy granular layer expansion during feeding. Adhesion energy varies depending on the zone of the exoskeleton tested; for instance, in the abdomen, adhesion is about twice that of the legs, which is consistent with a population of smaller dirt-grains adhered to the legs.

5. Conclusions

Regarding the structural materials of *M. spinolai*, they must be both soft to stretch significantly and hard to serve as a protective exoskeleton, which are contradictory requirements. *M. spinolai* achieved a highly expandable protective cuticle by introducing a dense network of wrinkles combined with pillars, both contributing to storing the exocuticle surface, which allows the cuticle to handle a considerable volume increase during feeding. The characterization of the mechanical properties of *M. spinolai* exoskeleton through atomic force spectroscopy provides important clues to understand its wrinkled structure, contrasted with confocal laser microscopy. Moreover, the use of a mechanical argument based on the minimization of total elastic energy, which considers the bending energy of the stiffer, thinner layer plus the stretching energy of the thicker, softer layer, leads to the prediction of a typical wrinkle size that is consistent with that observed in the insect, suggesting that the *M. spinolai* pattern results solely from mechanical instability.

Finally, we propose that the layer of grains acquired by *M. spinolai* after molting is a protection strategy, providing both camouflages to hide from both predators and prey, as well as an additional mechanical barrier. Our results show that grains are adhered to the exoskeleton through a low-energy adhesion glue that is highly stretchable and contains a limited viscous component, which allows for the easy expansion of both the granular layer and the exoskeleton during complete feeding. Thus, a sticky layer of grains may serve as an extremely resistant protective shield.

CRediT authorship contribution statement

Nicolás Padilla-Manzano: Writing – review & editing, Writing – original draft, Visualization, Validation, Software, Resources, Project administration, Methodology, Investigation, Formal analysis, Data curation, Conceptualization. **Lisa Shafroth:** Software, Resources, Investigation, Conceptualization. **Laura Tamayo:** Writing – review & editing, Writing – original draft, Validation, Supervision, Software, Resources, Investigation, Funding acquisition, Formal analysis. **Nicol Quiroga:** Writing – original draft, Methodology, Investigation. **Carezza Botto-Mahan:** Writing – review & editing, Writing – original draft, Validation, Supervision, Resources, Project administration, Methodology, Investigation, Funding acquisition, Formal analysis, Data curation, Conceptualization. **Francisco Melo:** Writing – review & editing, Writing – original draft, Visualization, Validation, Supervision, Software, Resources, Project administration, Methodology, Investigation, Funding acquisition, Formal analysis, Data curation, Conceptualization.

Funding

This research received partial financial assistance from Fondequip [EQM230061] ANID-FONDECYT [1221045], ANID-FONDECYT [1241498], ANID/ANILLO/ATE [230025], ANID-FONDECYT [1240984] and DICYT USACH [042331 MH].

Declaration of competing interest

The authors declare that they have no known competing financial interests or personal relationships that could have appeared to influence the work reported in this paper.

Acknowledgments

We express our gratitude to L. Caballero for valuable support in implementing nano-micro indentation tools, to A. Maine for assistance in acquiring AFM images, E. Sentis for technical aid, L. Saragoni for assistance in acquiring CLSM images, and E. San Juan, R. Medel and V. Valdés for their contributions in image acquisition. We acknowledge Beca EPEC Doctorado (N.P).

Appendix A. Supplementary data

Supplementary data to this article can be found online at https://doi.org/10.1016/j.matdes.2025.115277.

Data availability

Data will be made available on request.

References

[1] M.A. Meyers, J. McKittrick, P.-Y. Chen, Structural Biological Materials: critical Mechanics-Materials Connections, Science 339 (2013) 773–779, https://doi.org/10.1126/science.1220854.
[2] J.A. Nychka, M.M. Gentleman, Implications of wettability in biological materials science, JOM 62 (2010) 39–48, https://doi.org/10.1007/s11837-010-0107-6.
[3] S.E. Naleway, M.M. Porter, J. McKittrick, M.A. Meyers, Structural Design elements in Biological Materials: Application to Bioinspiration, Adv. Mater. 27 (2015) 5455–5476, https://doi.org/10.1002/adma.201502403.
[4] P. Egan, R. Sinko, P.R. LeDuc, S. Keten, The role of mechanics in biological and bio-inspired systems, Nat. Commun. 6 (2015) 7418, https://doi.org/10.1038/ncomms8418.
[5] F. Barthelat, Z. Yin, M.J. Buehler, Structure and mechanics of interfaces in biological materials, Nat. Rev. Mater. 1 (2016) 16007, https://doi.org/10.1038/natrevmats.2016.7.
[6] X. Zhao, J. Zhang, K.Y. Zhu, Chito-Protein Matrices in Arthropod Exoskeletons and Peritrophic Matrices, in: E. Cohen, H. Merzendorfer (Eds.), Extracellular Sugar-Based Biopolymers Matrices, Springer International Publishing, Cham, 2019, pp. 3–56, https://doi.org/10.1007/978-3-030-12919-4_1.
[7] P.-Y. Chen, A.-Y.-M. Lin, J. McKittrick, M.A. Meyers, Structure and mechanical properties of crab exoskeletons, Acta Biomater. 4 (2008) 587–596, https://doi.org/10.1016/j.actbio.2007.12.010.
[8] T. Inoue, S. Oka, T. Hara, Three-dimensional microstructure of robust claw of coconut crab, one of the largest terrestrial crustaceans, Mater. Des. 206 (2021) 109765, https://doi.org/10.1016/j.matdes.2021.109765.
[9] T. Inoue, T. Yoshihama, Exoskeletons of mud crabs, *Scylla serrata*, of different sizes: Body weight, surface morphology, internal tissue structure, and mechanical resistance, Mater. Des. 258 (2025) 114699, https://doi.org/10.1016/j.matdes.2025.114699.
[10] P. Romano, H. Fabritius, D. Raabe, The exoskeleton of the lobster *Homarus americanus* as an example of a smart anisotropic biological material, Acta Biomater. 3 (2007) 301–309, https://doi.org/10.1016/j.actbio.2006.10.003.
[11] S. Amini, M. Tadayon, J.Q.I. Chua, A. Miserez, Multi-scale structural design and biomechanics of the pistol shrimp snapper claw, Acta Biomater. 73 (2018) 449–457, https://doi.org/10.1016/j.actbio.2018.04.038.
[12] B. Reinhard, T. Weihmann, F.G. Barth, Measuring strain in the exoskeleton of spiders—virtues and caveats, Journal of Comparative Physiology: Neuroethology, Sensory, Neural, and Behavioral Physiology, A 207 (2021) 191–204, https://doi.org/10.1007/s00359-020-01458-y.
[13] A.B. Kesel, A. Martin, T. Seidl, Getting a grip on spider attachment: an AFM approach to microstructure adhesion in arthropods, Smart Mater. Struct. 13 (2004) 512, https://doi.org/10.1088/0964-1726/13/3/009.
[14] H. Zhang, I. Kellersztein, G. Freychet, M. Zhernenkov, H. Daniel Wagner, J. R. Greer, Chemo-mechanical-microstructural coupling in the tarsus exoskeleton of the scorpion *Scorpio palmatus*, Acta Biomaterialia 160 (2023) 176–186, https://doi.org/10.1016/j.actbio.2023.01.038.
[15] I. Kellersztein, S.R. Cohen, B. Bar-On, H.D. Wagner, The exoskeleton of scorpions' pincers: Structure and micro-mechanical properties, Acta Biomater. 94 (2019) 565–573, https://doi.org/10.1016/j.actbio.2019.06.036.
[16] S. Wood, J.D. Russell, On the Nature of the Calcium Carbonate in the Exoskeleton of the Woodlouse Oniscus asellus L (Isopoda, Oniscoidea), Crustaceana 53 (1987) 49–53.

[17] H. Khemaissia, M. Raimond, A. Ayari, R. Jelassi, C. Souty-Grosset, K. Nasri-Ammar, Cuticular differences of the exoskeleton relative to habitat preferences among three terrestrial isopods, Biologia 73 (2018) 477–483, https://doi.org/10.2478/s11756-018-0052-3.

[18] H. Peisker, J. Michels, S.N. Gorb, Evidence for a material gradient in the adhesive tarsal setae of the ladybird beetle Coccinella septempunctata, Nat. Commun. 4 (2013) 1661, https://doi.org/10.1038/ncomms2576.

[19] L.-Y. Wang, H. Rajabi, N. Ghoroubi, C.-P. Lin, S.N. Gorb, Biomechanical strategies underlying the Robust Body Armour of an Aposematic Weevil, Front. Physiol. 9 (2018), https://doi.org/10.3389/fphys.2018.01410.

[20] C. Li, S.N. Gorb, H. Rajabi, Cuticle sclerotization determines the difference between the elastic moduli of locust tibiae, Acta Biomater. 103 (2020) 189–195, https://doi.org/10.1016/j.actbio.2019.12.013.

[21] C. Li, S.N. Gorb, H. Rajabi, Biomechanical strategies to reach a compromise between stiffness and flexibility in hind femora of desert locusts, Acta Biomater. 134 (2021) 490–498, https://doi.org/10.1016/j.actbio.2021.07.030.

[22] T. Zeimet, S.N. Gorb, W. Krings, Morphology and material composition of raptorial foreleg cuticles in praying mantises Gongylus gongylodes and Sphodromantis lineola, Sci. Rep. 15 (2025) 20208, https://doi.org/10.1038/s41598-025-06427-6.

[23] A. Guarneri, M. Lorenzo, eds., Triatominae - The Biology of Chagas Disease Vectors, Springer International Publishing, Cham, 2021. doi:10.1007/978-3-030-64548-9.

[24] S.S. Catalá, F. Noireau, J.-P. Dujardin, 7 - Biology of Triatominae, in: J. Telleria, M. Tibayrenc (Eds.), American Trypanosomiasis Chagas Disease (second Edition), Elsevier, London, 2017, pp. 145–167, https://doi.org/10.1016/B978-0-12-801029-7.00007-1.

[25] J.A. de Fuentes-Vicente, A.E. Gutiérrez-Cabrera, A.L. Flores-Villegas, C. Lowenberger, G. Benelli, P.M. Salazar-Schettino, A. Córdoba-Aguilar, What makes an effective Chagas disease vector? Factors Underlying Trypanosoma Cruzi-Triatomine Interactions, Acta Tropica 183 (2018) 23–31, https://doi.org/10.1016/j.actatropica.2018.04.008.

[26] H. Lent, P.W. Wygodzinsky, Revision of the Triatominae (Hemiptera, Reduviidae), and their significance as vectors of Chagas' disease, Bulletin of the AMNH 163 (1979).

[27] J.R. Coura, P.A. Viñas, A.C. Junqueira, Ecoepidemiology, short history and control of Chagas disease in the endemic countries and the new challenge for non-endemic countries, Mem. Inst. Oswaldo Cruz 109 (2014) 856–862, https://doi.org/10.1590/0074-0276140236.

[28] E. San Juan, R. Araya-Donoso, A. Sandoval-Rodríguez, A. Yáñez-Meza, N. Quiroga, C. Botto-Mahan, Lizards and rabbits may increase Chagas infection risk in the Mediterranean-type ecosystem of South America, Sci. Rep. 10 (2020) 1853, https://doi.org/10.1038/s41598-020-59054-8.

[29] E. San Juan, R. Araya-Donoso, C. Sierra-Rosales, J.P. Correa, N. Quiroga, R. Campos-Soto, A. Solari, M. Llewellyn, A. Bacigalupo, C. Botto-Mahan, Humans as blood-feeding sources in sylvatic triatomines of Chile unveiled by next-generation sequencing, Parasites Vectors 16 (2023) 225, https://doi.org/10.1186/s13071-023-05841-x.

[30] C. Botto-Mahan, A. Bacigalupo, J.P. Correa, F.E. Fontúrbel, P.E. Cattan, A. Solari, Prevalence, infected density or individual probability of infection? Assessing vector infection risk in the wild transmission of Chagas disease, in: Proceedings of the Royal Society B: Biological Sciences 287, 2020, https://doi.org/10.1098/rspb.2019.3018.

[31] M. Canals, R. Solis, J. Valderas, M. Ehrenfeld, P.E. Cattan, Preliminary Studies on Temperature selection and activity Cycles of Triatoma infestans and T. spinolai (Heteroptera: Reduviidae), Chilean Vectors of Chagas' Disease, J. Med. Entomol. 34 (1997) 11–17, https://doi.org/10.1093/jmedent/34.1.11.

[32] P.A. Ramírez, A. González, C. Botto-Mahan, Masking Behavior by Mepraia spinolai (Hemiptera: Reduviidae): Anti-predator Defense and Life history Trade-offs, J. Insect Behav. 26 (2013) 592–602, https://doi.org/10.1007/s10905-012-9371-3.

[33] N. Quiroga, M.I. Muñoz, S.A. Pérez-Espinoza, M. Penna, C. Botto-Mahan, Stridulation in the wild kissing bug Mepraia spinolai: description of the stridulatory organ and vibratory disturbance signal, Bioacoustics 29 (2020) 266–279, https://doi.org/10.1080/09524622.2019.1603120.

[34] D. Estay-Olea, J.P. Correa, S. de Bona, A. Bacigalupo, N. Quiroga, E. San Juan, A. Solari, C. Botto-Mahan, *Trypanosoma cruzi* could affect wild triatomine approaching behaviour to humans by altering vector nutritional status: a field test, Acta Tropica 210 (2020) 105574, https://doi.org/10.1016/j.actatropica.2020.105574.

[35] L. Amorim, A. Santos, J.P. Nunes, J.C. Viana, Bioinspired approaches for toughening of fibre reinforced polymer composites, Mater. Des. 199 (2021) 109336, https://doi.org/10.1016/j.matdes.2020.109336.

[36] W. Krings, S.N. Gorb, Editorial: composite materials in biological and bioinspired systems, Interface Focus 14 (2024) 20240008, https://doi.org/10.1098/rsfs.2024.0008.

[37] Y. Zheng, J. Wang, J. Wang, Y. Li, Z. Jiang, Insect cuticle: a source of inspiration for biomimetic Interface material design, Colloid Interface Sci. Commun. 64 (2025) 100818, https://doi.org/10.1016/j.colcom.2025.100818.

[38] T.B.H. Schroeder, J. Houghtaling, B.D. Wilts, M. Mayer, It's not a bug, It's a Feature: Functional Materials in Insects, Adv. Mater. 30 (2018) 1705322, https://doi.org/10.1002/adma.201705322.

[39] B. Chen, D. Yin, W. Ye, S. Lin, J. Fan, J. Gou, Fiber-continuous panel–pillar structure in insect cuticle and biomimetic research, Mater. Des. 86 (2015) 686–691, https://doi.org/10.1016/j.matdes.2015.07.102.

[40] S.-M. Chen, S.-M. Wen, S.-C. Zhang, C.-X. Wang, S.-H. Yu, Biological and bioinspired Bouligand structural materials: recent advances and perspectives, Matter 7 (2024) 378–407, https://doi.org/10.1016/j.matt.2023.11.013.

[41] L. Bai, L. Liu, M. Esquivel, B.L. Tardy, S. Huan, X. Niu, S. Liu, G. Yang, Y. Fan, O. J. Rojas, Nanochitin: Chemistry, Structure, Assembly, and applications, Chem. Rev. 122 (2022) 11604–11674, https://doi.org/10.1021/acs.chemrev.2c00125.

[42] A. Miserez, J. Yu, P. Mohammadi, Protein-based Biological Materials: Molecular Design and Artificial Production, Chem. Rev. 123 (2023) 2049–2111, https://doi.org/10.1021/acs.chemrev.2c00621.

[43] F. Yuan, X.-X. Zhang, K. Wu, Z. Li, Y. Lin, X. Liang, Q. Yang, T. Liu, Damping chitin hydrogels by harnessing insect-cuticle-inspired hierarchical structures, CR-PHYS-SC 4 (2023), https://doi.org/10.1016/j.xcrp.2023.101644.

[44] R. Garrido, R. Campos-Soto, N. Quiroga, C. Botto-Mahan, Bloodmeal-stealing in wild-caught Mepraia spinolai (Hemiptera: Reduviidae), a sylvatic vector of Trypanosoma cruzi, Ecol. Entomol. 46 (2021) 681–683, https://doi.org/10.1111/een.12999.

[45] C. Botto-Mahan, Trypanosoma cruzi Induces Life-history Trait changes in the Wild kissing bug Mepraia spinolai: Implications for Parasite Transmission, Vector-Borne and Zoonotic Diseases 9 (2009) 505–510, https://doi.org/10.1089/vbz.2008.0003.

[46] J. Michels, S. n. Gorb, Detailed three-dimensional visualization of resilin in the exoskeleton of arthropods using confocal laser scanning microscopy, Journal of Microscopy 245 (2012) 1–16. doi:10.1111/j.1365-2818.2011.03523.x.

[47] N. Padilla-Manzano, S. Santander, T. Vera, E. Jara, L.F. Álvarez, B. Díaz, R. Bacchiega, J.C. Forero Oliveros, P. Santana, E. Hamm, M.D. Urzúa, L. Tamayo, Combined effect of the Core–Shell Structure and Variable Wettability in Polymer Fiber Membranes for dual and delayed Release of active Agents, ACS Appl, Polym. Mater. 6 (2024) 10436–10451, https://doi.org/10.1021/acsapm.4c01582.

[48] H.-J. Butt, B. Cappella, M. Kappl, Force measurements with the atomic force microscope: Technique, interpretation and applications, Surf. Sci. Rep. 59 (2005) 1–152, https://doi.org/10.1016/j.surfrep.2005.08.003.

[49] P.J. de Pablo, I.A.T. Schaap, F.C. MacKintosh, C.F. Schmidt, Deformation and Collapse of Microtubules on the Nanometer Scale, Phys. Rev. Lett. 91 (2003) 098101, https://doi.org/10.1103/PhysRevLett.91.098101.

[50] I.N. Sneddon, The relation between load and penetration in the axisymmetric boussinesq problem for a punch of arbitrary profile, Int. J. Eng. Sci. 3 (1965) 47–57, https://doi.org/10.1016/0020-7225(65)90019-4.

[51] J. Marthelot, B. Roman, J. Bico, J. Teisseire, D. Dalmas, F. Melo, Self-Replicating Cracks: a Collaborative Fracture Mode in Thin Films, Phys. Rev. Lett. 113 (2014) 085502, https://doi.org/10.1103/PhysRevLett.113.085502.

[52] J. Marthelot, J. Bico, F. Melo, B. Roman, A new failure mechanism in thin film by collaborative fracture and delamination: Interacting duos of cracks, J. Mech. Phys. Solids 84 (2015) 214–229, https://doi.org/10.1016/j.jmps.2015.07.010.

[53] X. Chen, J.W. Hutchinson, Herringbone Buckling patterns of Compressed Thin Films on Compliant Substrates, J. Appl. Mech. 71 (2004) 597–603, https://doi.org/10.1115/1.1756141.

[54] P. Kim, M. Abkarian, H.A. Stone, Hierarchical folding of elastic membranes under biaxial compressive stress, Nature Mater 10 (2011) 952–957, https://doi.org/10.1038/nmat3144.

[55] F. Brau, P. Damman, H. Diamant, T.A. Witten, Wrinkle to fold transition: influence of the substrate response, Soft Matter 9 (2013) 8177–8186, https://doi.org/10.1039/C3SM50655J.

[56] K.L. Johnson, Contact Mechanics, Cambridge University Press, 1987.

[57] M.J. Lehane, in: Managing the Blood Meal, Biology of Blood-Sucking Insects, Springer, Netherlands, Dordrecht, 1991, pp. 79–110, https://doi.org/10.1007/978-94-011-7953-9_6.

[58] J. Nattero, G. Leonhard, C.S. Rodríguez, L. Crocco, Influence of the quality and quantity of blood ingested on reproductive parameters and life-span in *Triatoma infestans* (Klug), Acta Trop. 119 (2011) 183–187, https://doi.org/10.1016/j.actatropica.2011.05.015.

[59] J. Nattero, C.S. Rodríguez, L. Crocco, Effects of blood meal source on food resource use and reproduction in Triatoma patagonica Del Ponte (Hemiptera, Reduviidae), J. Vector Ecol. 38 (2013) 127–133, https://doi.org/10.1111/j.1948-7134.2013.12018.x.

[60] A. Sharbidre, S. Sargar, H. Gogoi, R. Patil, Characterization of chitin content extracted from edible insect, Coridius nepalensis (Westwood, 1837) (Hemiptera: Dinidoridae), Int J Trop Insect Sci 41 (2021) 1893–1900. doi:10.1007/s42690-020-00386-3.

[61] A. Sánchez-Sánchez, M. Cerdán, J.D. Jordá, B. Amat, J. Cortina, Characterization of soil mineralogy by FTIR: application to the analysis of mineralogical changes in soils affected by vegetation patches, Plant Soil 439 (2019) 447–458, https://doi.org/10.1007/s11104-019-04061-6.

[62] P.B. Ramírez, F.J. Calderón, S.J. Fonte, F. Santibáñez, C.A. Bonilla, Spectral responses to labile organic carbon fractions as useful soil quality indicators across a climatic gradient, Ecol. Ind. 111 (2020) 106042, https://doi.org/10.1016/j.ecolind.2019.106042.

[63] P.I. Haris, D. Chapman, The conformational analysis of peptides using fourier transform IR spectroscopy, Biopolymers 37 (1995) 251–263, https://doi.org/10.1002/bip.360370404.

[64] V.A. Iconomidou, G.D. Chryssikos, V. Gionis, J.H. Willis, S.J. Hamodrakas, "Soft"-cuticle protein secondary structure as revealed by FT-Raman, ATR FT-IR and CD Spectroscopy, Insect Biochemistry and Molecular Biology 31 (2001) 877–885, https://doi.org/10.1016/S0965-1748(01)00033-9.

[65] D. Montroni, F. Sparla, S. Fermani, G. Falini, Influence of proteins on mechanical properties of a natural chitin-protein composite, Acta Biomater. 120 (2021) 81–90, https://doi.org/10.1016/j.actbio.2020.04.039.

[66] H.R. Hepburn, I. Joffe, Locust solid cuticle—A time sequence of mechanical properties, J. Insect Physiol. 20 (1974) 497–506, https://doi.org/10.1016/0022-1910(74)90158-9.

[67] M. Schmitt, T.H. Büscher, S.N. Gorb, H. Rajabi, How does a slender tibia resist buckling? effect of material, structural and geometric characteristics on buckling behaviour of the hindleg tibia in stick insect postembryonic development, J Exp Biol 221 (2018) jeb173047, https://doi.org/10.1242/jeb.173047.
[68] J. Rong, Y. Lin, Z. Sui, S. Wang, X. Wei, J. Xiao, D. Huang, Amorphous calcium phosphate in the pupal cuticle of *Bactrocera dorsalis* Hendel (Diptera: Tephritidae): a new discovery for reconsidering the mineralization of the insect cuticle, J. Insect Physiol. 119 (2019) 103964, https://doi.org/10.1016/j.jinsphys.2019.103964.
[69] J. Michels, E. Appel, S.N. Gorb, Functional diversity of resilin in Arthropoda, Beilstein J. Nanotechnol. 7 (2016) 1241–1259, https://doi.org/10.3762/bjnano.7.115.
[70] S.O. Andersen, T. Weis-Fogh, Resilin. A Rubberlike Protein in Arthropod Cuticle, in: J.W.L. Beament, J.E. Treherne, V.B. Wigglesworth (Eds.), Advances in Insect Physiology, Academic Press, 1964: pp. 1–65. doi:10.1016/S0065-2806(08)60071-5.
[71] F. Bäumler, S. Büsse, Resilin in the flight apparatus of Odonata (Insecta)—cap tendons and their biomechanical importance for flight, Biol. Lett. 15 (2019) 20190127, https://doi.org/10.1098/rsbl.2019.0127.
[72] J. Michels, S.N. Gorb, K. Reinhardt, Reduction of female copulatory damage by resilin represents evidence for tolerance in sexual conflict, J. R. Soc. Interface 12 (2015) 20141107, https://doi.org/10.1098/rsif.2014.1107.
[73] E. Appel, J. Michels, S.N. Gorb, Resilin in Insect Flight Systems, Adv. Funct. Mater. 34 (2024) 2215162, https://doi.org/10.1002/adfm.202215162.
[74] S.O. Andersen, Insect cuticular sclerotization: a review, Insect Biochem. Mol. Biol. 40 (2010) 166–178, https://doi.org/10.1016/j.ibmb.2009.10.007.
[75] L.-Y. Wang, M. Jafarpour, C.-P. Lin, E. Appel, S.N. Gorb, H. Rajabi, Endocuticle sclerotisation increases the mechanical stability of cuticle, Soft Matter 15 (2019) 8272–8278, https://doi.org/10.1039/C9SM01687B.
[76] K.K. Gadgey, A. Bahekar, STUDIES ON EXTRACTION METHODS OF CHITIN FROM CRAB SHELL AND INVESTIGATION OF ITS MECHANICAL PROPERTIES, IJMET 8 (2017) 220–231.
[77] K.F. Gauss, General Investigations of Curved Surfaces: Edited with an Introduction and notes by Peter Pesic, Courier Corporation (2013).
[78] Sk. Faruque Ahmed, S. Nagashima, J.Y. Lee, K.-R. Lee, K.-S. Kim, M.-W. Moon, Self-assembled folding of a biaxially compressed film on a compliant substrate, Carbon 76 (2014) 105–112. doi:10.1016/j.carbon.2014.04.056.